Phosphate group grafted twinned BiPO$_4$ with significantly enhanced photocatalytic activity: Synergistic effect of improved charge separation efficiency and redox ability

Yan Guo, Peifang Wang[*], Jin Qian, Yanhui Ao[*], Chao Wang, Jun Hou

Key Laboratory of Integrated Regulation and Resource Development on Shallow Lakes, Ministry of Education, College of Environment, Hohai University, No.1, Xikang road, Nanjing, 210098, China

ARTICLE INFO

ABSTRACT

The photocatalytic technology based on solar energy is a potential approach to mitigate environmental problem. The surface property of photocatalysts and the separation efficiency of photo-generated spatial charge are considerably important to enhance their photocatalytic activity in the decomposition of organic pollutants in wastewater. In this work, phosphate group grafted twinned BiPO$_4$ with surface phase junction were controllably synthesized by a facile two-step method. XRD results showed that two crystal phases of nMBIP and mMBIP were formed in the twinned BiPO$_4$. The formation of phase junction in BiPO$_4$ was also validated by HRTEM. XPS spectra confirmed that PO$_4^{3-}$ successfully grafted on the surface of the twinned BiPO$_4$. The apparent rate constants of the twinned BiPO$_4$ for degradation of methylene blue (MB) and carbamazepine (CBZ) improved 5.3 and 5.0 times respectively compared to pristine BiPO$_4$ because of the formed phase junction. After phosphate grafting on the surface of phase junction, the apparent rate constants for MB and CBZ degradation were further boosted, which were 3.0 and 5.2 times as high as that of twinned BiPO$_4$. The photocatalytic intermediates of CBZ were detected by HPLC-ESI-MS/MS, and a deductive degradation pathway of CBZ was proposed. Transient photocurrent responses, PL and Mott-Schottky analysis verified that the enhanced photocatalytic activity of phosphate group grafted twinned BiPO$_4$ with phase junction for the degradation of MB and CBZ was ascribed to faster transfer, efficient separation and improved redox ability of photo-induced charge carriers.

1. Introduction

Photocatalysis is one of the most ideal environment purification techniques because of its ability to mineralize refractory organics thoroughly by utilizing sunlight and its advantages of lower energy consumption, no secondary pollution, easy accessibility and so on. TiO$_2$, as a type of earliest discovered photocatalyst, has been investigated extensively [1–3]. Over the past few decades, besides the research of the traditional TiO$_2$-based photocatalytic materials, a large number of new-typed promising photocatalysts have also been developed [4–6].

In 2010, BiPO$_4$, a Bi-based oxy-acid salt photocatalyst, was detected to exhibit superior catalytic activity than P25 under UV light irradiation by Zhu et al [7]. But the low separation efficiency of photo-excited electrons and holes was still a major drawback for widespread application of BiPO$_4$. As a consequence, varying methods were taken to overcome the flaw, for example, forming hetero-junction structure via coupling with other semiconductors [8,9], doping with nonmetal [10]

and depositing noble metal [11]. All these strategies can bring about a high photocatalytic performance. In recent several years, semiconductor photocatalysts with phase junction has attracted plentiful studies since Li's group [12] put forward the concept of phase junction. The separation efficiency of charge carriers can also be boosted by the formed phase junction between different crystal phases in one semiconductor [13–16]. For BiPO$_4$, the crystal phase transformed from hexagonal BiPO$_4$ (HBIP) to monazite monoclinic BiPO$_4$ (nMBIP) and then to monoclinic BiPO$_4$ (mMBIP) through calcination. BiPO$_4$ with phase junction was verified to have enhanced photocatalytic activity due to efficient separation and transfer of electrons and holes [17].

On the other hand, it is generally known that photocatalytic reaction usually takes place on the surface of photocatalysts. Therefore, the surface properties of photocatalysts are crucial to enhance the photocatalytic activity for the degradation of organic pollutants. Recently, inorganic oxyanions such as phosphate had been used to modify photocatalysts and gained some achievements. Chen and co-workers [18] successfully synthesized phosphate group modified BiOBr with

---

enhanced activity. They found out that the enhanced activity can be ascribed to the higher charge separation efficiency caused by increasing ability of oxygen adsorption which accelerated the capture of photo-excited electrons. Another literature reported by Li et al. [19] showed that the positive holes would be trapped by negative field on the surface of BiOCl formed by phosphate groups modification. Therefore, carrier lifetime was prolonged and resulted in improved photocatalytic performance. Furthermore, mechanism on improvment of the separation efficiency of photogenerated charge carriers by phosphate modification was also expounded in TiO_2 [20] and $BiVO_4$ [21]. $BiPO_4$ was also reported to have enhanced photocatalytic performance through phosphate modification [23].

Therefore, we attempted to conceive a new idea to enhance the photocatalytic performance of $BiPO_4$ by combining the advantages of phase junction and phosphate modification. In the present study, phosphate-grafted twinned $BiPO_4$ nanorods with phase junction were synthesized by adjusting the ratio of Bi/P of $BiPO_4$ followed by calcining treatment at different temperatures. Meanwhile, the photocatalytic performance was assessed by decomposition of methylene blue (MB) and carbamazepine (CBZ, an antiepileptic drugs) under ultraviolet light irradiation. Subsequently, the mechanism for enhanced activity was discussed detailedly.

2. Experimental section

2.1. Synthesis of photocatalysts

Chemical solvents and reagents were purchased with analytical grade except chromatographically pure acetonitrile used in high performance liquid chromatography (HPLC). All chemicals were used directly without further purification. The water used in the whole experiment was ultrapure water.

Bare $BiPO_4$ and phosphate-grafted $BiPO_4$ were synthesized by a facile method with $Bi(NO_3)_3 \cdot 5H_2O$ and $NaH_2PO_4 \cdot 2H_2O$ as reactants. In a typical procedure, 4.85 g $Bi(NO_3)_3 \cdot 5H_2O$ was dissolved in 10% glycerin solution firstly, and then an amount of $NaH_2PO_4 \cdot 2H_2O$ was added into the solution keeping vigorous stirring for 1 h. Anterior to drying at 120 °C for 12 h, the white solid matter was obtained after centrifugation and washed with plenty of ethanol and water. For the synthesis of pristine $BiPO_4$ defined as $BP_{1.0}$, the molar ratios of $NaH_2PO_4 \cdot 2H_2O$ to $Bi(NO_3)_3 \cdot 5H_2O$ were controlled at 1.0. In order to synthesize phosphate-grafted $BiPO_4$ samples, the molar ratios of $NaH_2PO_4 \cdot 2H_2O$ to $Bi(NO_3)_3 \cdot 5H_2O$ were controlled in the range of 1.1–5.0, and the corresponding products were defined as BP_x, where x refers to the molar ratios of $NaH_2PO_4 \cdot 2H_2O$ to $Bi(NO_3)_3 \cdot 5H_2O$.

Phosphate-grafted $BiPO_4$ with various crystal phases were prepared by calcining BP_x at 400 °C, 500 °C, 600 °C for 6 h in an atmosphere furnace in air, which were marked as BP_x-400, BP_x-500 and BP_x-600 respectively.

2.2. Characterization of photocatalysts

The phase structure properties of the fabricated photocatalysts were enucleated by the powder X-ray diffraction (XRD, Rigaku, SmartLab) scanning over the range of 2θ between 5° and 55°. The transmission electron microscopy (TEM, JEOL) and high resolution transmission electron microscopy (HRTEM, JEM-2100) were carried out to clarify the morphologies and microstructures of the samples. X-ray photoelectron spectrometer (Thermo, ESCALAB250Xi) was employed to acquire the X-ray photoelectron spectroscopy (XPS). Wavelength dispersive X-ray fluorescence (WD-XRF) was executed on the ZSX Primus-II. The UV–vis diffuse reflectance spectra (DRS) of the as-synthesized samples were drawn on UV–vis spectrophotometer (Shimadzu, UV3600). Photoluminescence (PL) spectra were recorded on a fluorescence spectrophotometer (Hitachi, F-7000) to validate the separation efficiency of photo-excited electron-hole pairs. In addition, trapping

experiment was implemented to ascertain the active species in the photocatalytic reaction. In order to investigate the electric properties of monazite monoclinic $BiPO_4$ (nMBIP) and monoclinic $BiPO_4$ (mMBIP), pure nMBIP and mMBIP were also fabricated based on previous literature [24].

2.3. Photocatalytic activity

The photocatalytic activities of the obtained photocatalysts were estimated on the photo-degradation of methylene blue (MB, 5 mg/L) as a probe reaction under ultraviolet (UV) light irradiation. The photocatalytic degradation process of MB was summed up in the following steps. 50 mg as-prepared photocatalyst was added into 100 mL of MB aqueous solution. Antecedent to exposure to UV light (a 300 W xenon lamp (Zhongjiaojinyuan, CEL-HXUV300)), the suspension was ultrasonically treated for several minutes and was stirred in dark for 90 min to obtain adsorption-desorption equilibrium. During the process of photocatalytic reaction, 1.5 mL of suspension was collected and analyzed after centrifugation. UV–vis spectrophotometer (Shimadzu, UV3600) was hired to determine the concentrations of collected methylene blue. The flux of incident light was measured to be about 4.9 Lm.

The photocatalytic degradation experiments of carbamazepine (CBZ) were carried out with the same procedure. The catalysts in sampled suspension were dislodged by filtration with a 0.22-μm membrane, and then the filtrate was analyzed by HPLC quantitatively.

2.4. Chemical analysis

The concentration of sampled CBZ was quantified by HPLC (Agilent 1260 series) equipped with a UV detector at an excited wavelength of 210 nm, with a column temperature of 25 °C. Elution was carried out with water and acetonitrile (45:55%, v/v) at a constant flow rate of 1.0 mL/min and the injection volume of 20 μL. CBZ was analyzed by the external standard method and its retention time was 2.24 min.

The degradation intermediates of CBZ were qualitatively analyzed by the mass spectrometer LC-ESI-MS/MS (Agilent 1290/6460 Triple Quad LC/MS) in electrospray positive ion (ESI +) mode with acetonitrile (solvent A) and ultrapure water with 0.1%v formic acid (solvent B) as mobile phase. The transformation intermediates were well separated according to a gradient elution and the procedure as follows: the initial conditions for 90% A and 10% B hold 5 min, then B was increased to 70% in 25 min and hold for 10 min, and finally return to the initial conditions in 10 min. The degradation products of CBZ were monitored and analyzed by recording mass spectra in full scan mode with a detection time of 50 min for qualitative analysis.

The concentrations of phosphorus element in solution were detected by double beam UV–vis spectrophotometer according to the molybdenum blue method that includes a digestion step (5% Potassium persulfate, 120 °C, 150 kPa for 30 min) and a color development step (10% ascorbic acid solution and molybdate solution) [25]. Specifically, three parallel experiments and controlled trials were carried out synchronously.

2.5. Photoelectrochemical measurement

Photoelectric response performance of as-prepared photocatalysts signified by photocurrent measurements was measured in a three-electrode system using a CHI660D electrochemical station (Chenhua Instruments). The working, counter and reference electrodes were sample films, platinum plate and Ag/AgCl, respectively. Detailedly, the working electrodes were prepared as following procedure. 20 mg of catalyst powder was dispersed on 2 mL of absolute ethanol by ultrasonic processing. Then, obtained homogeneous mixing suspension was coated onto the conductive side of fluoride tin oxide (FTO) glass. In order to increase adhesion, the electrodes were placed into an oven and
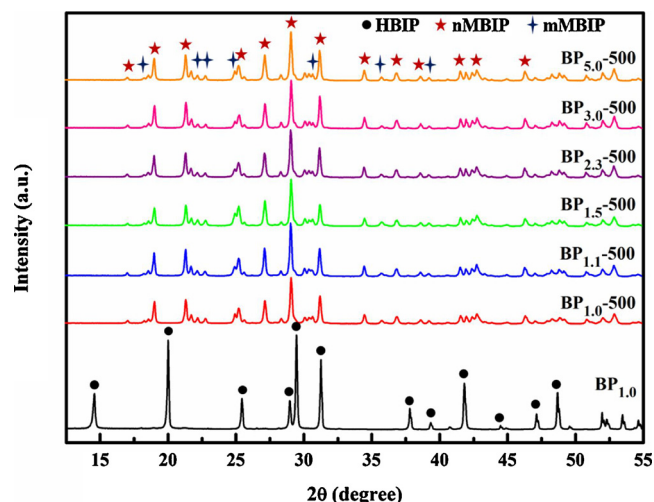
Fig. 1. XRD patterns of pristine $BiPO_4$ and phosphate-grafted $BiPO_4$ calcined at 500 °C.

dried at 120 °C for 3 h. Furthermore, 0.1 M Na_2SO_4 was served as the electrolyte. A 250 W mercury lamp (Instrumental Corporation of Beijing Normal University) was used as the UV light source, and the photoelectric response were recorded under evenly spaced intervals of the alternant light and dark. The Mott-Schottky analysis with frequencies of 300 Hz, 500 Hz and 1000 Hz and an amplitude of 5 mV was conducted with the same equipment under dark condition. The measured potentials versus Ag/AgCl were converted to the normal hydrogen electrode (NHE) scale by the equation $E_{NHE} = E_{Ag/AgCl} + 0.197$[26].

3. Results and discussions

3.1. Characterization

The XRD patterns of bare $BiPO_4$ and phosphate-grafted $BiPO_4$ calcined at 500 ∘C were presented in Fig. 1 to confirm the phase and purity of the products. All the detected diffraction peaks of $BP_{1.0}$ were in accorded with the characteristic peaks of pure HBIP ($P3_121$, JCPDS 015-0766) [27] completely. With the advent of nMBIP ($P2_1/n$, JCPDS 015-0767) [28] and mMBIP ($P2_1/m$, JCPDFS 43-0637) [24], the peaks of HBIP disappeared absolutely for $BP_{1.0}$-500. As shown in the figure, BP_x-500 exhibited uniform diffraction peaks as well as $BP_{1.0}$-500, suggesting the successful formation of phase-junction structure between nMBIP and mMBIP at calcination temperature of 500 °C. No impurity peaks were discovered in all the patterns, signifying the high purity of the obtained photocatalysts. The products possessed high crystallinity because of their intense and sharp diffraction peaks [29].

The microstructures were investigated via TEM characterization and the obtained typical images are shown in Fig. 2. As we can see from Fig. 2(a,c), morphology and size of $BP_{1.0}$-500 were similar to that of $BP_{1.0}$. After grafting with phosphate, apparent differences can be found between $BP_{3.0}$-500 and $BP_{1.0}$-500, such as coarser surface, smaller diameter and shorter length. It can be ascribed to the fact that the grain growth of $BiPO_4$ was inhibited by phosphate (PO_4^{3-}). Meanwhile, HR-TEM images displayed in Fig. 2(b,d and f) further illuminated the transformation of $BiPO_4$ phase structure. For $BP_{1.0}$, the clear crystal lattice with interplanar spacing of 0.307 nm matched to the (111) lattice plane of HBIP ($P3_121$, JCPDS 015-0766) (Fig. 2b). $BP_{1.0}$-500 showed the (012) lattice plane of nMBIP ($P2_1/n$, JCPDS 015-0767) with characteristic spacing of 0.286 nm and the (210) lattice plane of mMBIP ($P2_1/m$, JCPDS 43-0637) with characteristic spacing of 0.229 nm. Similarly, the phosphate-grafted sample, $BP_{3.0}$-500, possessed two kinds of crystal planes which corresponded to nMBIP and mMBIP

respectively. The characteristic results of HR-TEM convincingly demonstrated the successful transition of phase structure from HBIP to nMBIP and mMBIP under 500 °C calcination. Thus, the surface-phase junction structure was distinctly formed between nMBIP and mMBIP in $BP_{1.0}$-500 and $BP_{3.0}$-500.

The DRS spectra were employed to investigate the optical absorption properties. As is well known, $BiPO_4$ has a wide optical band gap, and it has no any optical absorption with wavelength beyond 340 nm (shown in Fig. 3). Furthermore, a steeply increased optical absorption was found at around 280 nm. Hence, it can only be excited by ultraviolet light irradiation. The Tauc's plot was used to calculate the optical band gap energies of semiconductors and expressed as the equation [30]: $ahv = A(hv - Eg)^{n/2}$. Where a, h, v, Eg and A are absorption coefficient, Planck constant, light frequency, band gap energy, and a constant, respectively. n is determined by distinguishing the direct (n = 1) or indirect (n = 4) optical transition of a semiconductor. Based on literatures reported previously, the n values of $BiPO_4$ was 4 [31]. From the plot of $(ahv)^{1/2}$ versus (hv) shown in the inset of Fig. 3, the energy band gap of $BP_{1.0}$, $BP_{1.0}$-500 and $BP_{3.0}$-500 were approximately 4.23 eV, 4.06 eV and 4.40 eV, respectively.

The compositions and chemical states of different elements in $BP_{1.0}$-500 and $BP_{3.0}$-500 simultaneously were identified by the XPS. Bi, P and O were all detected in $BP_{1.0}$-500 and $BP_{3.0}$-500. Fig. 4a–c were drawn to compare the high-resolution XPS spectra of Bi 4f, P 2p and O 1s on the surface of the catalysts respectively. For Bi in $BP_{1.0}$-500 and $BP_{3.0}$-500 as shown in Fig. 4a, the broad Bi 4f principally consists of a Bi $4f_{5/2}$ peak at around 164.3 eV and a Bi $4f_{7/2}$ at around 159.2 eV, both of which are ascribed to trivalent bismuth (Bi^{3+}) in $BiPO_4$ [32,33]. As shown in Fig. 4b, a single peak at approximately 132.9 eV can be detected in the P 2p region of the samples, corresponding to pentavalent phosphorus-oxidation state (P^{5+}) of P–O bond in PO_4^{3-} [34,35]. In Fig. 4c, the curve of the O 1s can be fitted to three peaks at approximately 530.3 eV, 530.9 eV, 531.9 eV which can be assigned to the Bi–O, P–O, and OH group, respectively [23,36]. Remarkably, for $BP_{3.0}$-500, the binding energy of Bi 4f and P 2p were weaker than that in $BP_{1.0}$-500, suggesting that the electron density increased because of the PO_4^{3-} grafting on the surface of $BiPO_4$, which is in conformity with previous literature [23]. The surface negative electrostatic fields caused by PO_4^{3-} can attract holes and repel electrons, which was beneficial to promote charge separation.

The real atomic ratios between phosphorus and bismuth in the different PO_4^{3-}-grafted $BiPO_4$ samples after calcination at 500 °C were further determined by the WD-XRF analysis. The results were presented in Table S1. Obviously, the actual quantities of modified PO_4^{3-} in calcined $BiPO_4$ were all significantly smaller than initial atom ratio during the synthesis process. In addition, the real atomic ratios between P and Bi were gradually increased as the increasing of added amount of $NaH_2PO_4·2H_2O$.

3.2. Photocatalytic activity

The photocatalytic activities of the obtained catalysts were estimated by the photo-decomposition of MB as a probe reaction under UV light irradiation($\lambda < 400$ nm). The adsorption percents of MB by various photocatalysts are shown in Table S2. There were no obvious difference on the adsorption performance in different phosphate group grafted twinned $BiPO_4$ samples. Hence, the enhanced photocatalytic activity of phosphate group grafted twinned $BiPO_4$ was not dependent on their adsorption properties principally. The degradation reaction of MB was in conformity with the pseudo first-order kinetics [37,38], and the preliminary results are shown in Fig. 5. As demonstrated in Fig. 5a, the degradation percent of MB is only 20% for $BP_{1.0}$ without calcination. After calcination at different temperature, the photocatalytic performance of $BP_{1.0}$ first improved and then reduced with calcination temperature increased from 400 °C to 600 °C. The maximum photocatalytic activity is observed for $BP_{1.0}$-500 which is consistent with the
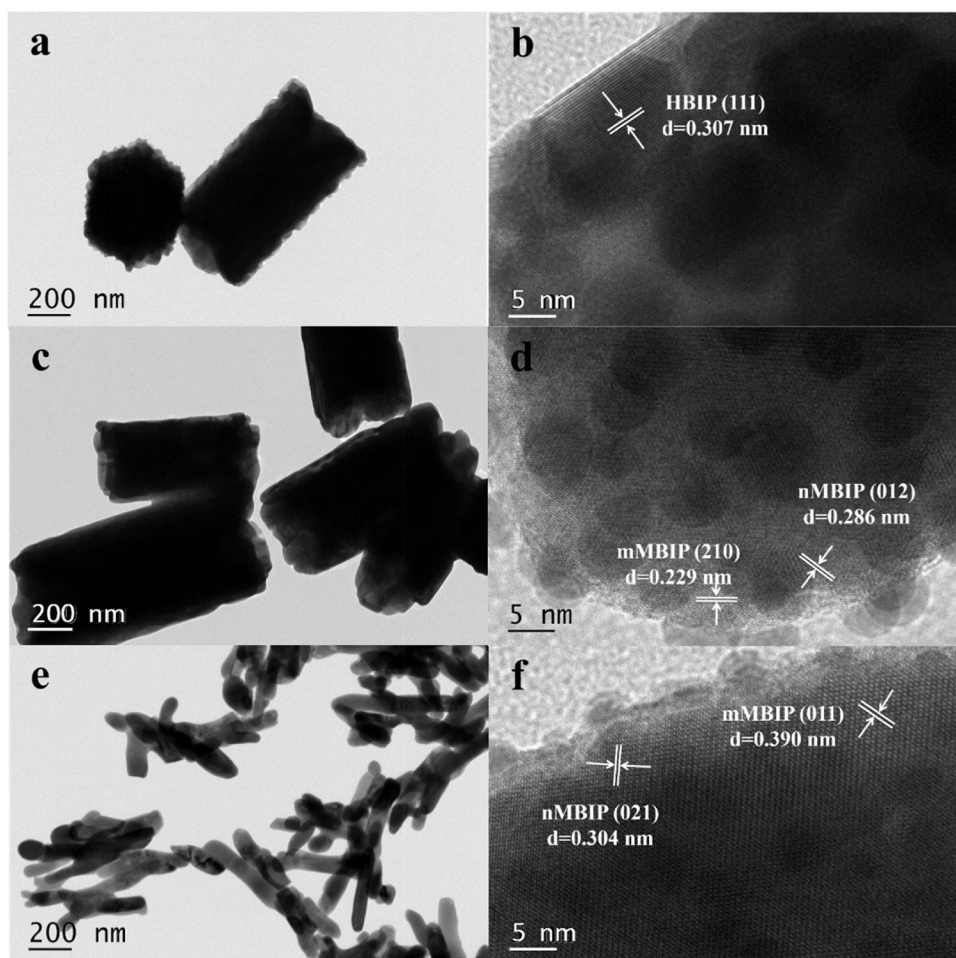
Fig. 2. Low-magnification and high-resolution TEM images of $BP_{1.0}$ (a,b), $BP_{1.0}$-500 (c,d) and $BP_{3.0}$-500 (e,f).
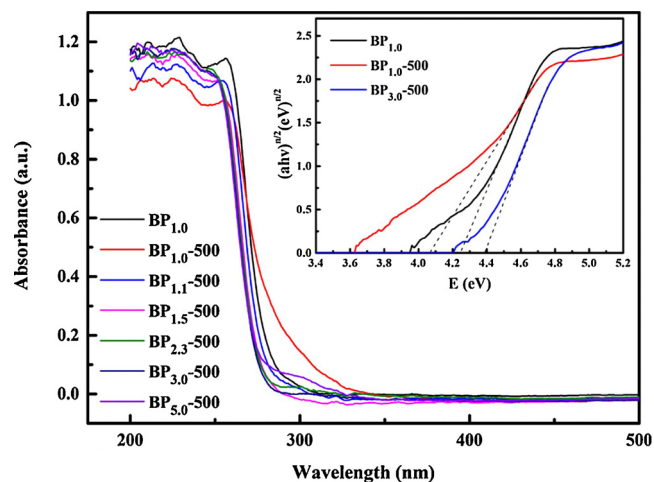

Fig. 3. UV–vis diffuse reflectance spectra for different samples with inset the optical band gap of $BP_{1.0}$, $BP_{1.0}$-500 and $BP_{3.0}$-500.

reported literature [17], and its apparent rate constant k reaches 0.046 min^{-1} which is 5.3 times as high as that of $BP_{1.0}$. That phenomenon may be ascribed to the formation of phase junction between nMBIP and mMBIP, which induces to efficient separation of photo-generated charge carriers. Thus, the enhancement of photocatalytic activity for BiPO$_4$ via phase junction is resultful.

To investigate the effect of phosphate modification on the photo-catalytic property of twinned $BP_{1.0}$, the photocatalytic degradation of

MB by phosphate-grafted BiPO$_4$ nanorods with phase junction was also conducted, and the obtained results are shown in Fig. 5(b–h). According to the results, photocatalytic performance of these modified samples exhibits analogical regularity with $BP_{1.0}$ under different calcination temperature. Thus, it can be further confirmed the photocatalytic performance could be effectively enhanced via phase junction formed on the BiPO$_4$. Furthermore, all the as-prepared samples with surface grafting PO_4^{3-} emerge the best photocatalytic performance when the calcination temperature reaches to 500 °C. The apparent rate constant k of BP_x-500 (x from 1.0 to 5.0) for MB degradation are expressed in Fig. 6. The corresponding values of k are calculated to be 0.0088, 0.046, 0.060, 0.082, 0.13, 0.14 and 0.087 min^{-1} for $BP_{1.0}$, $BP_{1.0}$-500, $BP_{1.1}$-500, $BP_{1.5}$-500, $BP_{2.3}$-500, $BP_{3.0}$-500 and $BP_{5.0}$-500, respectively. As we can clearly see in the figure, BP_x-500 (x from 1.0 to 5.0) all exhibit higher photocatalytic performances than that of $BP_{1.0}$-500 and $BP_{1.0}$. In addition, the k value of $BP_{3.0}$-500 is the highest in all samples which is about 15.9 and 3.0 times as high as that of $BP_{1.0}$ and $BP_{1.0}$-500, respectively. The control of quantitative ratio of nMBIP and mMBIP could be realized for $BP_{3.0}$ indirectly via calcining at different temperatures which were adjacent to 500 °C (i.e. 450, 475, 525 and 550 °C). Among them (Fig. S2), the highest performance was still detected on $BP_{3.0}$ calcined at 500 °C for MB degradation. Thus, the optimal quantitative ratio of nMBIP and mMBIP was identified on $BP_{3.0}$-500.

As we know, carbamazepine (CBZ) as an antiepileptic drugs is difficult to be biochemical decomposed in natural aquatic environment because of the symmetrical aromatic heterocyclic structure [39,40]. With the feature of voracious consumption, biological accumulation, ecological hazard and persistence, carbamazepine has been paid wide spread attention by researchers [41–43]. For the purpose of judging the
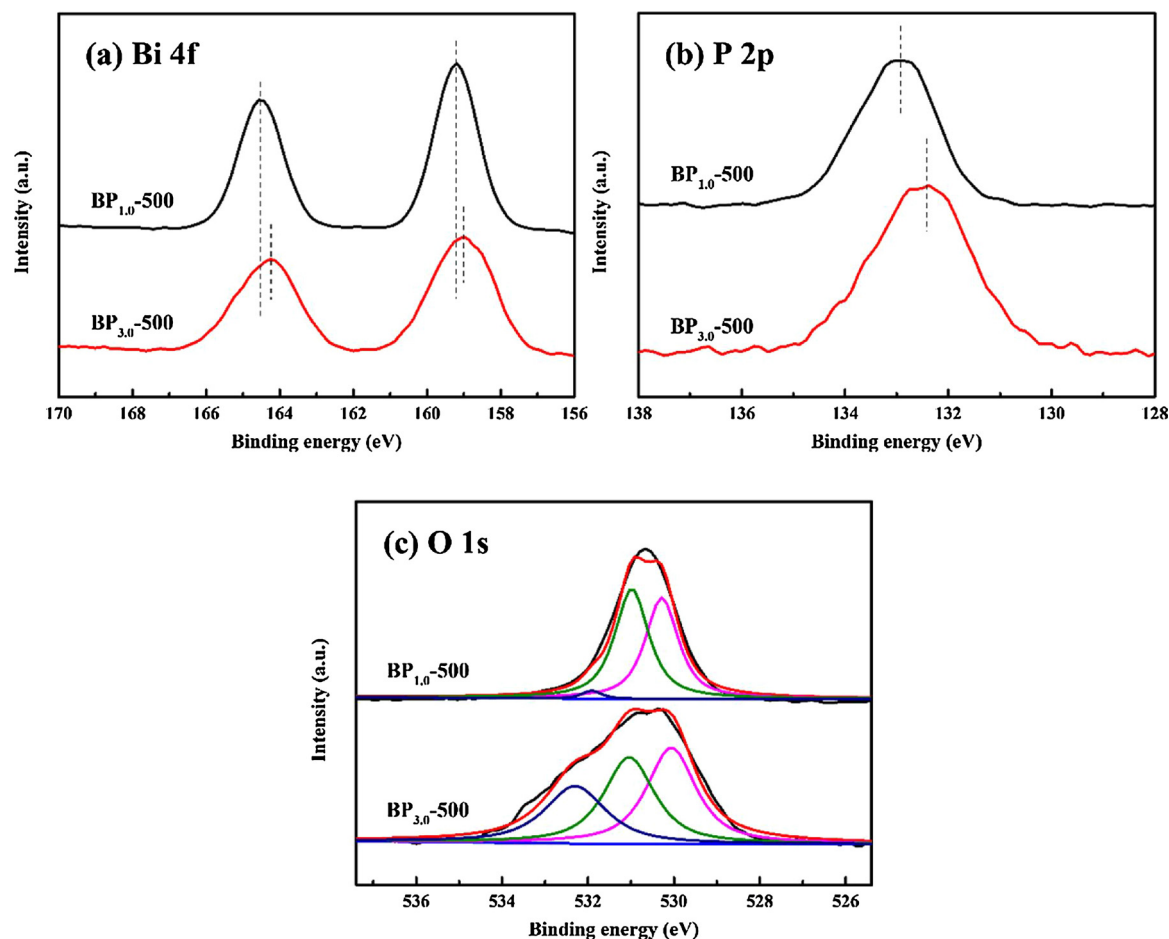
Fig. 4. High-resolution XPS spectra of the BP$_{1.0}$-500 and BP$_{3.0}$-500: (a) Bi 4f, (b) P 2p, (c) O 1s.

photocatalytic degradation ability for non-dye pollutant, CBZ (5 mg/L) was chosen as target pollutant and degraded by BP$_{1.0}$, BP$_{1.0}$-500 and BP$_{3.0}$-500. It can be seen from Fig. 7a that the degradation percent of CBZ by BP$_{1.0}$ is very low. Similar with the situation for MB degradation, after the formation of phase junction structure and modification with phosphate, BP$_{3.0}$-500 display better photocatalytic performance than BP$_{1.0}$. 79% of CBZ was decomposed by BP$_{1.0}$-500 in 30 min and nearly all CBZ was degraded by BP$_{3.0}$-500 in 20 min. The HPLC chromatograms of carbamazepine degradation over BP$_{3.0}$-500 at different time intervals were presented in Fig. S2. The Langmuir–Hinshelwood (L–H) kinetic model with pseudo-first-order was applied to evaluate the degradation efficiency of CBZ. The plots of ln(C$_0$/C) versus the reaction time (t) and corresponding apparent rate constant k are presented in Fig. 7b. The high correlation coefficients (R > 0.99) of all the fitted curves reveal that the degradation process of CBZ over different catalysts are in line with pseudo-first-order kinetic [44]. As is illustrated in the inset of Fig. 7b, the values of k are noted in the sequence of BP$_{3.0}$-500 > BP$_{1.0}$-500 > BP$_{1.0}$, which is in accordance with that of MB degradation. The photocatalytic activity of BP$_{1.0}$-500 has a five-fold enhancement compared with BP$_{1.0}$. Moreover, the k of BP$_{3.0}$-500 is 5.2 times as high as that of BP$_{1.0}$-500 and 26.0 times as high as that of BP$_{1.0}$, respectively. All the above results demonstrated the synergistic effect of phase junction structure and phosphate modification enhanced photocatalytic activity of BiPO$_4$ simultaneously.

In order to assess the stability of the phosphate group grafted on the surface of twinned BiPO$_4$, the P fractions were measured in the colorless solution after photocatalytic reaction over BP$_{1.0}$-500 and BP$_{3.0}$-500, respectively. The results showed that little phosphorus was detected in the solution after the photocatalytic reaction. By calculation, the

detected P fraction in colorless solution account for only 0.37% of total P for BP$_{3.0}$-500. The results indicated that the phosphate group grafted twinned BiPO$_4$ is stable in the photocatalytic process.

3.3. Degradation pathway of CBZ by BP$_{3.0}$-500

According to LC–ESI–MS/MS analysis results, the structure of intermediates and possible degradation pathway of CBZ (m/z = 237 g/mol) by BP$_{3.0}$-500 were proposed in Fig.8. The mass spectra of the degraded CBZ over BP$_{3.0}$-500 in typical HPLC-MS chromatogram were supplemented in Fig. S3. First of all, alkene double bond of CBZ was vulnerable to attack by ·OH radical due to its higher frontier electron density (FED) which is likely to conduct hydroxylation. Hence, CBZ was transferred into intermediate P1 (hydroxy CBZ, m/z = 253 g/mol) and P2 (epoxy CBZ, m/z = 253 g/mol) [45]. Besides, intermediate P1 was further hydroxylated to generate P3 (dihydroxy CBZ, m/z = 271) and P4 (trihydroxy CBZ, m/z = 287) which may be further degraded via gradual ring cleavage [46]. As for intermediate P2, it might be further oxidized by ·O$_2^-$ and photo-induced h$^+$ to convert into P5 (m/z = 267 g/mol) and P8 (m/z = 253 g/mol) that involved in cleavage reaction and ring contraction reaction respectively [47]. Interestingly enough, P3 might be generated by a hydrolysis step from P2 [47,48]. After aldehyde oxidation reaction in P5, P6 (m/z = 301 g/mol) was produced and further transferred to P7 (m/z = 259 g/mol) ascribed to deamination reaction [49]. Alternatively, product P8 underwent several successive steps including deamination and dehydroxylation to generate P9 (m/z = 180 g/mol) [39,50]. It can be speculated that P4, P7 and P9 could be further oxidized and finally mineralized into harmless CO$_2$ and H$_2$O via ring-rupturing reaction by oxidizing ·OH,

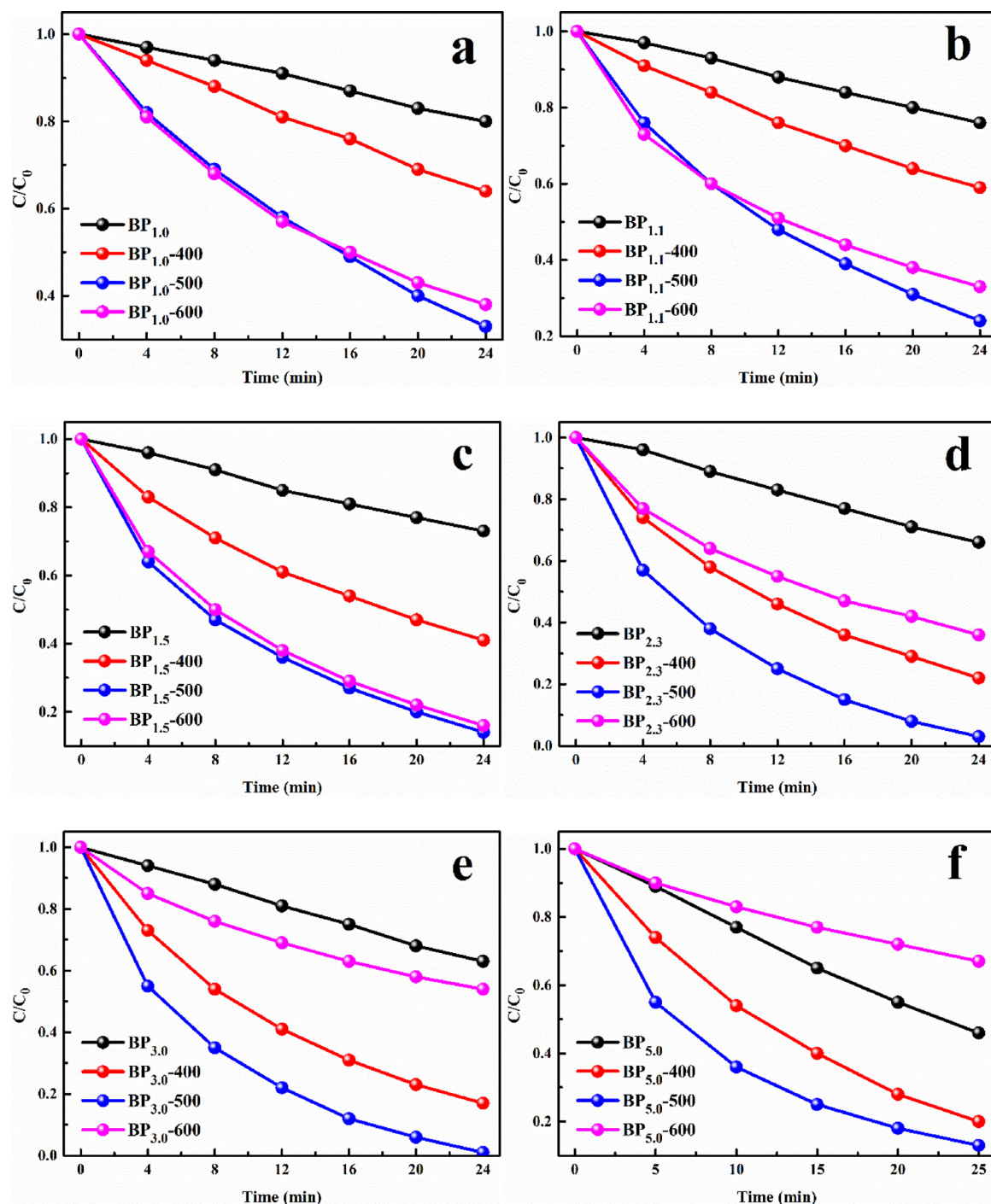**Fig. 5.** Photocatalytic degradation of MB for pristine BiPO$_4$ and phosphate-grafted BiPO$_4$ calcined at different temperature respectively.

h$^+$ and ·O$_2^-$.

3.4. Mechanism of the enhanced photocatalytic activity for phosphate-grafted BiPO$_4$ with phase junction structure

Generally, the transfer rate, separation efficiency and redox ability of photo-excited electrons and holes determined the photocatalytic performance of catalysts. Transient photocurrent responses, photoluminescence (PL) and Mott-Schottky analysis were employed to investigate these three factors.

The transient photocurrent response, as an indicator of electron transfer rate, was measured under UV light for BP$_{1.0}$, BP$_{1.0}$-500 and BP$_{3.0}$-500, and the obtained results are shown in Fig. 9. All the photocurrents were stable and reversible at light-on and light-off. As expected, BP$_{1.0}$ exhibited a minimum of photocurrent intensity. It can also be seen that the photocurrent intensity of BP$_{3.0}$-500 is about 3.5 and 2 as high as that of BP$_{1.0}$ and BP$_{1.0}$-500, respectively. Accordingly, BP$_{3.0}$-500 hold the fastest electron transfer rate and the longest lifetime of photo-induced charge carrier [51].

The separation of photo-excited electrons and holes can be further clarified by photoluminescence (PL) spectra with an emission peak at about 397 nm showed in Fig. 10. The excitation wavelength of BiPO$_4$ was identified as 250 nm. It can be seen that the emission intensity decreases gradually from BP$_{1.0}$ to BP$_{1.0}$-500 to BP$_{3.0}$-500. It is well known that the weaker intensity means lower recombination probability of photo-induced electron-hole pairs [52]. Thus, it can be
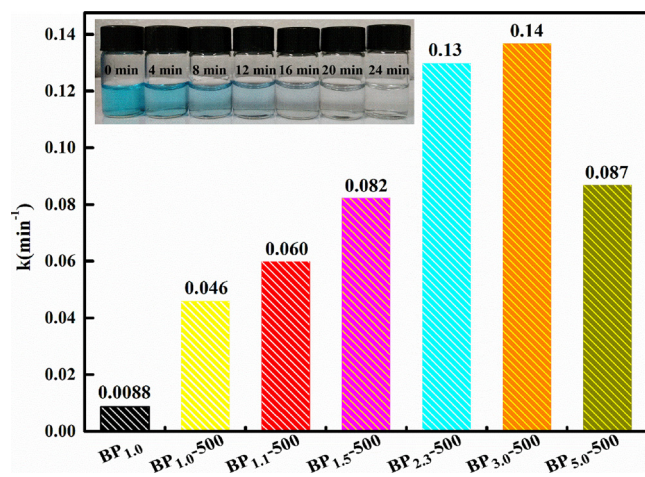
Fig. 6. The histogram of the apparent rate constant k of different photocatalysts for the degradation of MB, inset: the apparent change of the collected and centrifuged suspension of BP$_{3.0}$-500.
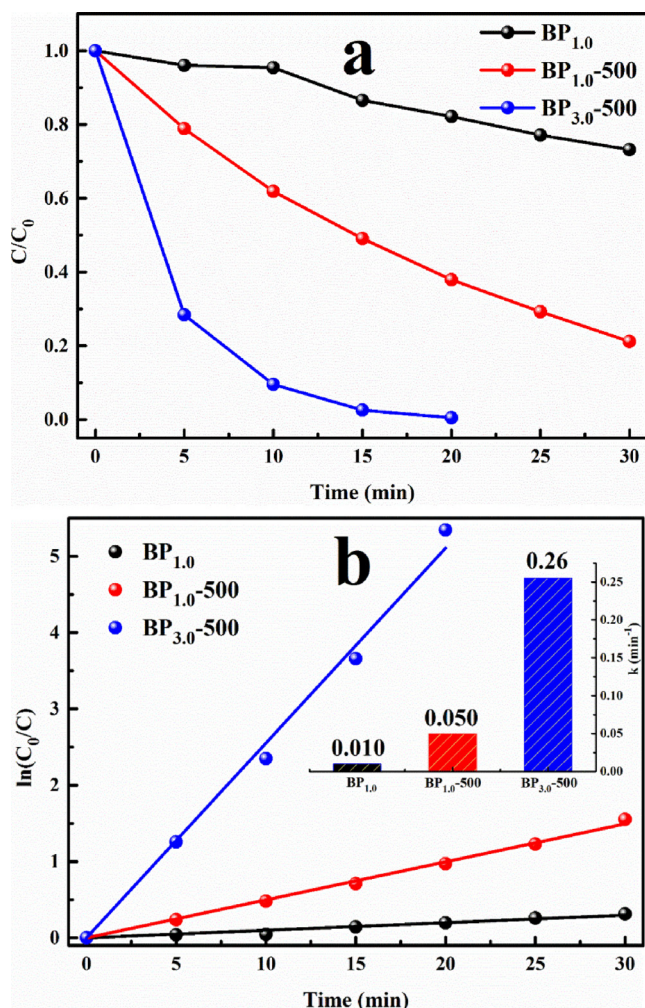

Fig. 7. (a) Photocatalytic decomposition of CBZ for photolysis, BP$_{1.0}$, BP$_{1.0}$-500 and BP$_{3.0}$-500 under ultraviolet radiation, (b) the corresponding kinetic curves with the histogram for corresponding apparent rate constant inset.

deduced that the recombination rate follows the order: BP$_{1.0}$ > BP$_{1.0}$-500 > BP$_{3.0}$-500, while the photocatalytic performance follows the opposite order. Judging from the transient photocurrent response plot and photoluminescence spectra simultaneously, it can be inferred that

the phase junction and phosphate modification synergistically facilitated the charge transfer and separation which induced favorable photocatalysis.
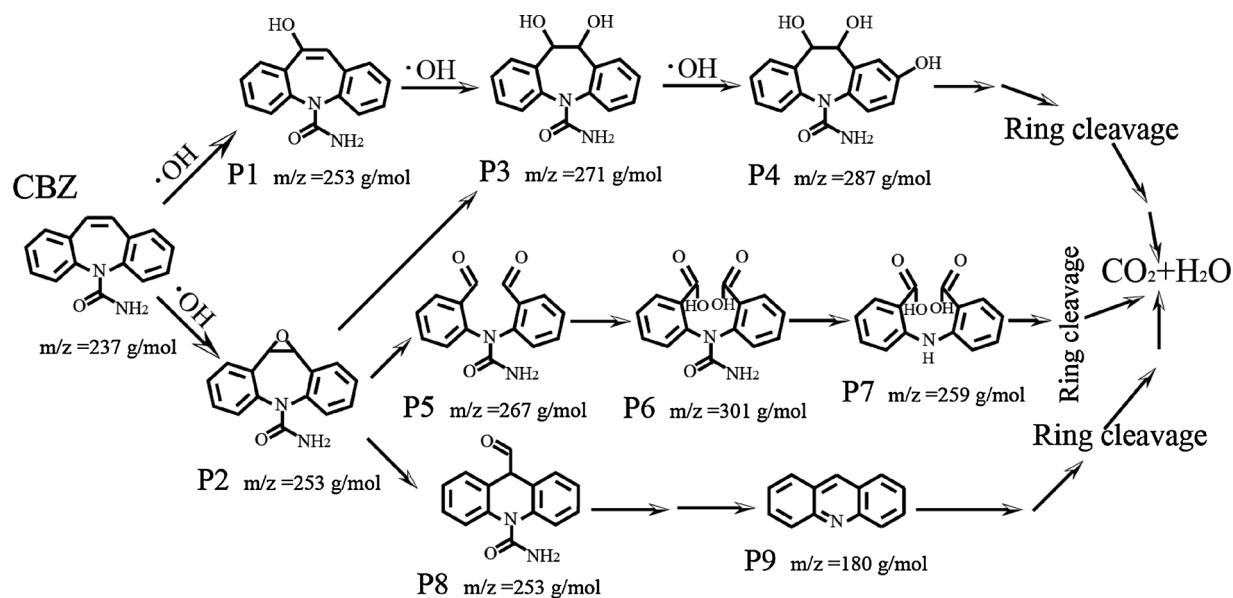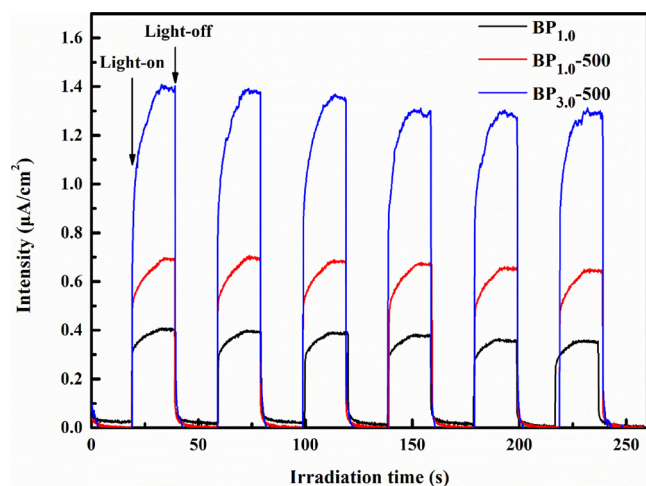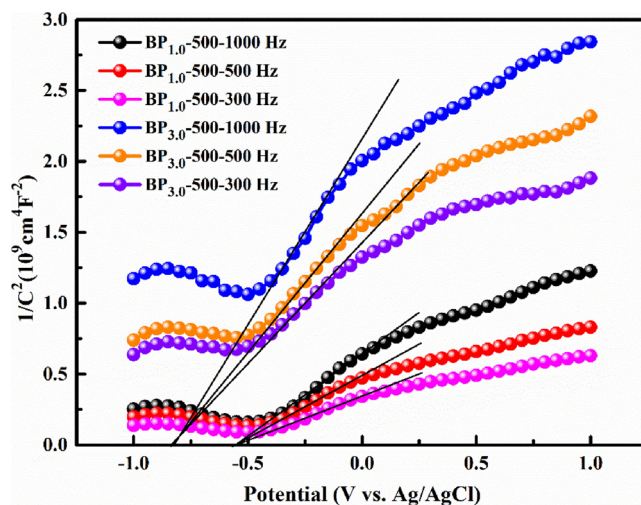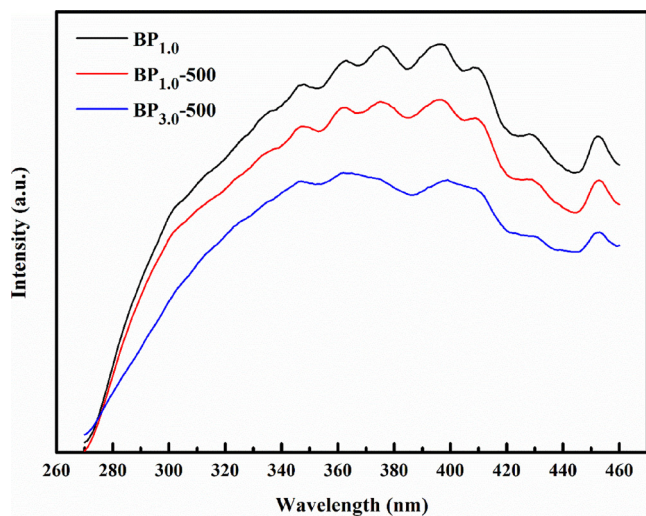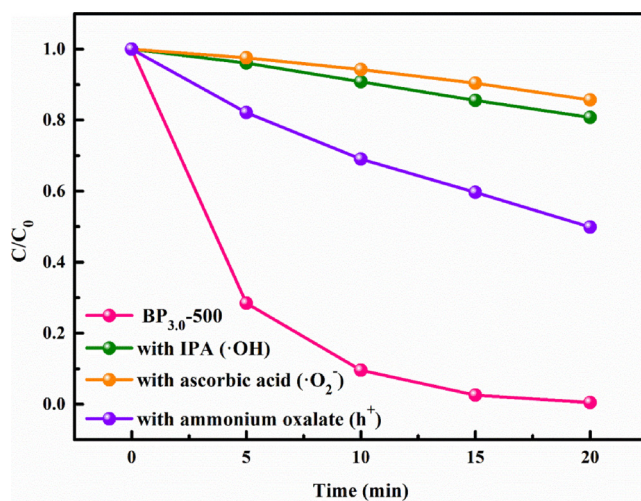
The Mott-Schottky analysis of BP$_{1.0}$-500 and BP$_{3.0}$-500 under dark conditions was implemented and the results were exhibited in Fig. 11. The positive slope of the fitted curves implied that BiPO$_4$ was n-type semiconductor [26]. The flat-band potential (E$_{fb}$) evaluated by the X-intercepts of the plot were approximately −0.54 and −0.82 V vs. Ag/AgCl (−0.34 and −0.62 V vs. NHE) for BP$_{1.0}$-500 and BP$_{3.0}$-500. It can see from Fig. 11 that the flat-band potential of the plot was same for one catalysts with different frequencies [53]. For an n-type semiconductor, the E$_{fb}$ is always regarded as the conduction-band potential [54]. Hence, according to the bandgap energies of 4.06 eV and 4.40 eV obtained from DRS experiments, the conduction and valence band edges were estimated to be −0.34 V (CB), +3.72 V (VB) and −0.62 V, +3.78 V for BP$_{1.0}$-500 and BP$_{3.0}$-500. Distinctly, the CB and VB edges of BP$_{3.0}$-500 occurred 0.28 V of upper shift and 0.06 V lower shift compared with that of BP$_{1.0}$-500, respectively. It is well known that the more negative CB position and more positive VB position of means more powerful redox ability which can give rise to the enhancement of photocatalytic performance.

With reference to the above characterization results, we concluded the following reasons for the enhanced photocatalytic degradation performance for phosphate-grafted BiPO$_4$ with phase junction in contrast to bare BiPO$_4$: 1) the formation of phase junction between two phase of BiPO$_4$ (nMBIP and mMBIP) boosted high mobility, ultrafast charge-carrier separation and transport; 2) the negative charge, on the BiPO$_4$ surface, generated by phosphate(PO$_4^{3-}$) surface modification can attract holes and repel electrons, which make further separation of photo-excited charge carriers and benefits photocatalytic activity; 3) the more negative conduction band edge potential and more positive valence band of phosphate-grafted BiPO$_4$ with phase junction structure compared with bare BiPO$_4$, which enhanced redox ability of photo-generated electrons-hole pairs and was conducive to photocatalytic decomposition of pollutants.

In order to ascertain the main active species generated during the photocatalytic degradation of CBZ, trapping experiments were conducted and the results are shown in Fig. 12. Isopropyl alcohol (IPA, scavengers of ·OH radical), ascorbic acid (VC, ·O$_2^-$ radical) and ammonium oxalate (h$^+$ radical) were added in the solution of CBZ during the photocatalytic process by BP$_{3.0}$-500. The decay of CBZ was appreciable prohibited with the addition of IPA or VC, indicating ·OH and ·O$_2^-$ were equally crucial active species. Moreover, degradation of CBZ was feebly depressed by ammonium oxalate, which revealed that h$^+$ served as synergistic active species but not as the most critical active species.

The proposed reaction mechanism for the photocatalytic degradation of carbamazepine over BP$_{3.0}$-500 under ultraviolet light irradiation was shown in Fig. 13. The band-gap energies of nMBIP and mMBIP were determined to be about 3.94 eV and 4.34 eV respectively from the inset profiles of the DRS spectra drawn in Fig. S4. As exhibited in the Mott-Schottky plots of nMBIP and mMBIP (Fig. S5), the flat-band potential (E$_{fb}$) of nMBIP was higher than that of mMBIP. Hence, the E$_{CB}$ of nMBIP and mMBIP were −0.65 and −0.61 V vs. NHE, and corresponding E$_{VB}$ were calculated to be 3.29 and 3.73 V vs. NHE depending on the value of band-gap energies. The CB and VB edge potential of nMBIP and mMBIP were determined and exhibited in Fig. 13. Under ultraviolet light irradiation, photo-induced electron would transfer from the CB of nMBIP to that of mMBIP due to the more negative E$_{CB}$ of nMBIP. And then, the electron reduced O$_2$ molecule adsorbed on the surface of photocatalyst into ·O$_2^-$ radical because the CB edge potential of BP$_{3.0}$-500 (−0.62 eV) was more negative than the redox potential of O$_2$/·O$_2$- (−0.33 eV). In the meantime, the holes migrated in an opposite path on the VB between nMBIP and mMBIP, resulting in an efficient separation of electrons and holes. Soon afterwards, the holes on the VB of nMBIP were attracted to the surface of catalyst by surface-

Fig. 8. Proposed degradation pathway of CBZ in the presence of BP$_{3.0}$-500.

Fig. 9. Transient photocurrent responses of BP$_{1.0}$, BP$_{1.0}$-500 and BP$_{3.0}$-500.

Fig. 11. Mott-Schottky plots of BP$_{1.0}$-500 and BP$_{3.0}$-500.

Fig. 10. Photoluminescence spectra of BP$_{1.0}$, BP$_{1.0}$-500 and BP$_{3.0}$-500.

Fig. 12. The plot of photocatalytic removal of carbamazepine over BP$_{3.0}$-500 with the addition of various scavenger under UV light irradiation.
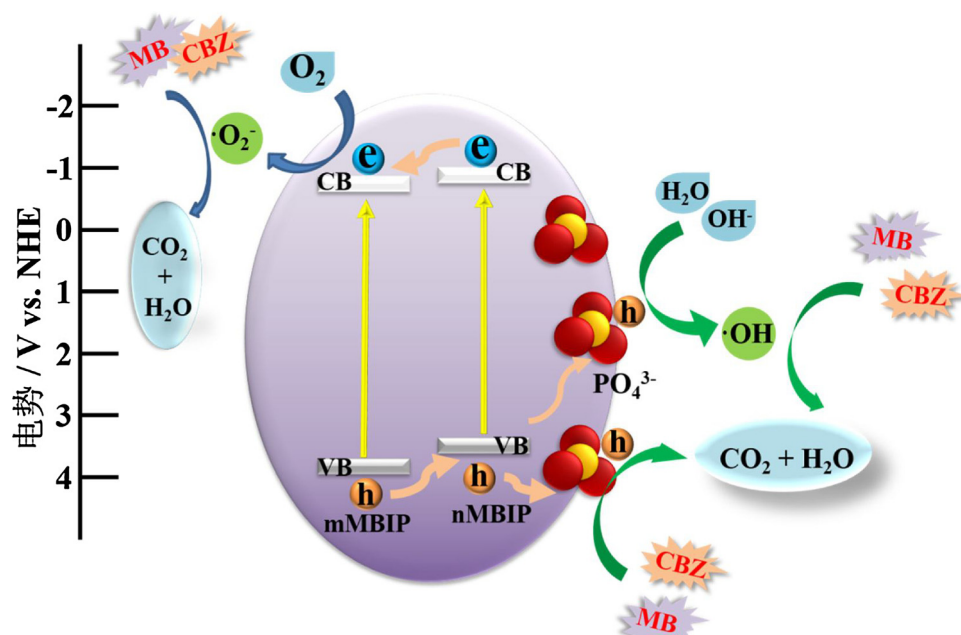
Fig. 13. Schematic illustrations of the photocatalytic degradation mechanism of MB and CBZ over the phosphate-grafted BiPO$_4$ with phase junction under UV light irradiation.

grafted phosphate anions. As a consequence, the recombination of photo-excited charge carriers were restrained efficiently. Meanwhile, the generated holes would partly react with H$_2$O or OH$^-$ to form ·OH radical, as the VB edge potential of BP$_{3.0}$-500 (+3.78 eV) was more positive than the potential of ·OH/H$_2$O (+2.68 eV) and ·OH/OH- (+1.99 eV). The produced ·O$_2^-$, ·OH radical and holes participated in the photocatalytic degradation reaction of carbamazepine, which in line with the trapping experiment results.

4. Conclusions

To sum up, the formation of phase junction and surface modification with phosphate anions endowed BiPO$_4$ with superior photocatalytic performances for the degradation of a colored dye MB and a common psychiatric drug (carbamazepine) in contrast to bare BiPO$_4$ and twinned BiPO$_4$ with phase junction under UV light irradiation. Besides, BP$_{3.0}$-500 exhibited optimum photocatalytic performance among all the catalysts. Based on the characterization results, it testified that synergistic effect between phase junction and PO$_4^{3-}$ modification can boost the transfer of photo-generated electron-hole pairs and restrain their recombination. Modification with PO$_4^{3-}$ of BiPO$_4$ with junction could affect the position of energy band and consequently improve the redox ability compared to the unmodified one. Furthermore, ·O$_2$-, ·OH and h$^+$ were all detected to take part in the reaction for photocatalytic degradation of organics. Based on HPLC-ESI-MS/MS results, the degradation products were identified and a deductive degradation pathway of CBZ in the presence of BP$_{3.0}$-500 was proposed. This study provided a good example to design high efficient photocatalysts through combination of homogenous junction with surface modification.

Acknowledgements

We are grateful for grants from National Science Funds for Creative Research Groups of China (No.51421006), Natural Science Foundation of China (51679063),The Fundamental Research Funds for The Central Universities (2018B14514) the Key Program of National Natural Science Foundation of China (No. 91647206), the National Science Fundation of China for Excellent Young Scholars (No. 51422902), the

National Key Plan for Research and Development of China (2016YFC0502203), Fundamental Research Funds (No. 2016B43814), and PAPD.

Appendix A. Supplementary data

Supplementary material related to this article can be found, in the online version, at doi:https://doi.org/10.1016/j.apcatb.2018.04.036.

References

[1] H. Tong, S.X. Ouyang, Y.P. Bi, N. Umezawa, M. Oshikiri, J.H. Ye, Nano-photo-catalytic materials: possibilities and challenges, Adv. Mater. 24 (2) (2012) 229–251.
[2] J. Schneider, M. Matsuoka, M. Takeuchi, J.L. Zhang, Y. Horiuchi, M. Anpo, D.W. Bahnemann, Understanding TiO$_2$ photocatalysis: mechanisms and materials, Chem. Rev. 114 (19) (2014) 9919–9986.
[3] Y. Ma, X.L. Wang, Y.S. Jia, X.B. Chen, H.X. Han, C. Li, Titanium dioxide-based nanomaterials for photocatalytic fuel generations, Chem. Rev. 114 (19) (2014) 9987–10043.
[4] S.W. Cao, J.X. Low, J.G. Yu, M. Jaroniec, Polymeric photocatalysts based on graphitic carbon nitride, Adv. Mater. 27 (13) (2015) 2150–2176.
[5] X. Yang, H. Li, W. Zhang, M.X. Sun, L.Q. Li, N. Xu, J.D. Wu, J. Sun, High visible photoelectrochemical activity of Ag nanoparticle-sandwiched CdS/Ag/ZnO nanorods, Acs Appl. Mater. Interfaces 9 (1) (2017) 658–667.
[6] R.J. Hou, Y. Gao, H.J. Zhu, G.X. Yang, W.H. Liu, Y.N. Huo, Z.L. Xie, H.X. Li, Coupling system of Ag/BiOBr photocatalysis and direct contact membrane distillation for complete purification of N-containing dye wastewater, Chem. Eng. J. 317 (2017) 386–393.
[7] C.S. Pan, Y.F. Zhu, New type of BiPO$_4$ oxy-acid salt photocatalyst with high photocatalytic activity on degradation of dye, Environ. Sci. Technol. 44 (14) (2010) 5570–5574.
[8] S. Obregón, Y.F. Zhang, G. Colón, Cascade charge separation mechanism by ternary heterostructured BiPO$_4$/TiO$_2$/g-C$_3$N$_4$ photocatalyst, Appl. Catal. B Environ. 184 (2016) 96–103.
[9] G.Q. Tan, L.N. She, T. Liu, C. Xu, H.J. Ren, A. Xia, Ultrasonic chemical synthesis of hybrid mpg-C$_3$N$_4$/BiPO$_4$ heterostructured photocatalysts with improved visible light photocatalytic activity, Appl. Catal. B Environ. 207 (2017) 120–133.
[10] Y.F. Liu, Y.H. Lv, Y.Y. Zhu, D. Liu, R.L. Zong, Y.F. Zhu, Fluorine mediated photocatalytic activity of BiPO$_4$, Appl. Catal. B Environ. 147 (14) (2014) 851–857.
[11] P. Zhang, H.H. Yu, J.J. Li, H. Zhao, B.L. Zhu, W.P. Huang, S.M. Zhang, Au/BiPO$_4$ nanorod catalysts: synthesis, characterization and their catalytic performance for CO oxidation, Rsc Adv. 6 (19) (2016) 15304–15312.
[12] J. Zhang, Q. Xu, Z.C. Feng, M.J. Li, C. Li, Importance of the relationship between surface phases and photocatalytic activity of TiO$_2$, Angew. Chem. 47 (9) (2008) 1766–1769.
[13] Y.S. Li, Z.L. Tang, J.Y. Zhang, Z.T. Zhang, Fabrication of vertical orthorhombic/hexagonal tungsten oxide phase junction with high photocatalytic performance, Appl. Catal. B Environ. 207 (2017) 207–217.

[14] J. Cheng, J. Feng, W. Pan, Enhanced photocatalytic activity in electrospun bismuth vanadate nanofibers with phase junction, Acs Appl. Mater. Interfaces 7 (18) (2015) 9638–9644.

[15] J.G. Hou, C. Yang, Z. Wang, W.L. Zhou, S.Q. Jiao, H.M. Zhu, In situ synthesis of α–β phase heterojunction on Bi_2O_3 nanowires with exceptional visible-light photocatalytic performance, Appl. Catal. B Environ. 142 (3) (2013) 504–511.

[16] X. Wang, Q. Xu, M.R. Li, S. Shen, X.L. Wang, Y.C. Wang, Z.C. Feng, J.Y. Shi, H.X. Han, C. Li, Photocatalytic overall water splitting promoted by an alpha-beta phase Junction on Ga_2O_3, Angew. Chem.-Int. Ed. 51 (52) (2012) 13089–13092.

[17] Y.Y. Zhu, Y.F. Liu, Y.H. Lv, Q. Ling, D. Liu, Y.F. Zhu, Enhancement of photocatalytic activity for $BiPO_4$ via phase junction, J. Mater. Chem. A 2 (32) (2014) 13041–13048.

[18] S.Y. Chen, R. Yan, X.L. Zhang, K. Hu, Z.J. Li, M. Humayun, Y. Qu, L.Q. Jing, Photogenerated electron modulation to dominantly induce efficient 2,4-dichlorophenol degradation on BiOBr nanoplates with different phosphate modification, Appl. Catal. B-Environ. 209 (2017) 320–328.

[19] Z.J. Li, Y. Qu, K. Hu, M. Humayun, S.Y. Chen, L.Q. Jing, Improved photoelectrocatalytic activities of BiOCl with high stability for water oxidation and MO degradation by coupling RGO and modifying phosphate groups to prolong carrier lifetime, Appl. Catal. B-Environ. 203 (2017) 355–362.

[20] L.Q. Jing, J. Zhou, J.R. Durrant, J.W. Tang, D.N. Liu, H.G. Fu, Dynamics of photogenerated charges in the phosphate modified TiO_2 and the enhanced activity for photoelectrochemical water splitting, Energy Environ. Sci. 5 (4) (2012) 6552–6558.

[21] M.Z. Xie, J. Bian, M. Humayun, Y. Qu, Y.J. Feng, L.Q. Jing, The promotion effect of surface negative electrostatic field on the photogenerated charge separation of $BiVO_4$ and its contribution to the enhanced PEC water oxidation, Chem. Commun. 51 (14) (2015) 2821–2823.

[23] Y. Li, Y.W. Wang, Y. Huang, J.J. Cao, W.K. Ho, S.C. Lee, C.M. Fan, Controllable synthesis of phosphate-modified $BiPO_4$ nanorods with high photocatalytic activity: surface hydroxyl groups concentrations effects, Rsc Adv. 5 (121) (2015) 99712–99721.

[24] C.S. Pan, D. Li, X.G. Ma, Y. Chen, Y.F. Zhu, Effects of distortion of PO_4 tetrahedron on the photocatalytic performances of $BiPO_4$, Catal. Sci. Technol. 1 (8) (2011) 1399–1405.

[25] J. Murphy, J.P. Riley, A modified single solution method for the determination of phosphate in natural waters, Anal. Chim. Acta 27 (00) (1962) 31–36.

[26] D.A. Reddy, H. Park, R. Ma, D.P. Kumar, M. Lim, T.K. Kim, Heterostructured WS_2-MoS_2 ultrathin nanosheets integrated on CdS nanorods to promote charge separation and migration and improve solar-driven photocatalytic hydrogen evolution, Chemsuschem 10 (7) (2017) 1563–1570.

[27] Z.S. Li, S.Y. Yang, J.M. Zhou, D.H. Li, X.F. Zhou, C.Y. Ge, Y.P. Fang, Novel mesoporous g-C_3N_4 and $BiPO_4$ nanorods hybrid architectures and their enhanced visible-light-driven photocatalytic performances, Chem. Eng. J. 241 (2014) 344–351.

[28] C.C. Fu, G.S. Li, M.L. Zhao, L.S. Yang, Z. Jing, L.P. Li, Solvent-driven room-temperature synthesis of nanoparticles $BiPO_4$:Eu^{3+}, Inorg. Chem. 51 (10) (2012) 5869–5800.

[29] Y.H. Ao, K.D. Wang, P.F. Wang, C. Wang, J. Hou, Synthesis of novel 2D-2D p-n heterojunction BiOBr/$La_2Ti_2O_7$ composite photocatalyst with enhanced photocatalytic performance under both UV and visible light irradiation, Appl. Catal. B Environ. 194 (2016) 157–168.

[30] S. Kamimura, T. Miyazaki, M. Zhang, Y.Q. Li, T. Tsubota, T. Ohno, (Au@Ag)@Au double shell nanoparticles loaded on rutile TiO_2 for photocatalytic decomposition of 2-propanol under visible light irradiation, Appl. Catal. B-Environ. 180 (2016) 255–262.

[31] Z.H. Wu, J. Liu, Q.Y. Tian, W. Wu, Efficient visible light formaldehyde oxidation with 2D p-n heterostructure of BiOBr/$BiPO_4$ nanosheets at room temperature, Acs Sustain. Chem. Eng. 5 (6) (2017) 5008–5017.

[32] H. Xu, Y.G. Xu, H.M. Li, J.X. Xia, J. Xiong, S. Yin, C.J. Huang, H.L. Wan, Synthesis, characterization and photocatalytic property of AgBr/$BiPO_4$ heterojunction photocatalyst, Dalton Trans. 41 (12) (2012) 3387–3394.

[33] Y.N. Huo, R.J. Hou, X.F. Chen, H.B. Yin, Y. Gao, H.X. Li, BiOBr visible-light photocatalytic films in a rotating disk reactor for the degradation of organics, J. Mater. Chem. A 3 (28) (2015) 14801–14808.

[34] M.H. Fulekar, A. Singh, D.P. Dutta, M. Roy, A. Ballal, A.K. Tyagi, Ag incorporated nano $BiPO_4$: sonochemical synthesis, characterization and improved visible light photocatalytic properties, Rsc Adv. 4 (20) (2014) 10097–10107.

[35] Z.G. Chen, X.L. Chen, J. Di, Y.L. Liu, S. Yin, J.X. Xia, H.M. Li, Graphene-like boron nitride modified bismuth phosphate materials for boosting photocatalytic degradation of enrofloxacin, J. Colloid Interface Sci. 492 (2017) 51–60.

[36] B. Pan, Y. Wang, Y.Y. Liang, S.J. Luo, W.Y. Su, X.X. Wang, Nanocomposite of $BiPO_4$ and reduced graphene oxide as an efficient photocatalyst for hydrogen evolution, Int. J. Hydrogen Energy 39 (25) (2014) 13527–13533.

[37] Y.H. Ao, L.Y. Xu, P.F. Wang, C. Wang, J. Hou, J. Qian, Preparation of CdS nanoparticle loaded flower-like $Bi_2O_2CO_3$ heterojunction photocatalysts with enhanced visible light photocatalytic activity, Dalton Trans. 44 (25) (2015) 11321–11330.

[38] Y.M. He, L.H. Zhang, M.H. Fan, X.X. Wang, M.L. Walbridge, Q.Y. Nong, Y. Wu, L.H. Zhao, Z-scheme SnO_2-x/g-C_3N_4 composite as an efficient photocatalyst for dye degradation and photocatalytic CO_2 reduction, Sol. Energy Mater. Sol. Cells 137 (2015) 175–184.

[39] J. Xu, L. Li, C.S. Guo, Y. Zhang, W. Meng, Photocatalytic degradation of carbamazepine by tailored $BiPO_4$: efficiency, intermediates and pathway, Appl. Catal. B-Environ. 130 (2013) 285–292.

[40] Y.B. Ding, G.L. Zhang, X.R. Wang, L.H. Zhu, H.Q. Tang, Chemical and photocatalytic oxidative degradation of carbamazepine by using metastable Bi^{3+} self-doped $NaBiO_3$ nanosheets as a bifunctional material, Appl. Catal. B Environ. 202 (2017) 528–538.

[41] H. Gulyas, M.K. Ogun, W. Meyer, M. Reich, R. Otterpohl, Inadequacy of carbamazepine-spiked model wastewaters for testing photocatalysis efficiency, Sci. Total Environ. 542 (2016) 612–619.

[42] T.E. Doll, F.H. Frimmel, Kinetic study of photocatalytic degradation of carbamazepine, clofibric acid, iomeprol and iopromide assisted by different TiO_2 materials - determination of intermediates and reaction pathways, Water Res. 38 (4) (2004) 955–964.

[43] A. Jelic, I. Michael, A. Achilleos, E. Hapeshi, D. Lambropoulou, S. Perez, M. Petrovic, D. Fatta-Kassinos, D. Barcelo, Transformation products and reaction pathways of carbamazepine during photocatalytic and sonophotocatalytic treatment, J. Hazard. Mater. 263 (2013) 177–186.

[44] M.C. Hu, Z.H. Yao, K.N. Hui, K.S. Hui, Novel mechanistic view of catalytic ozonation of gaseous toluene by dual-site kinetic modelling, Chem. Eng. J. 308 (2017) 710–718.

[45] D.P. Mohapatra, S.K. Brar, R. Daghrir, R.D. Tyagi, P. Picard, R.Y. Surampalli, P. Drogui, Photocatalytic degradation of carbamazepine in wastewater by using a new class of whey-stabilized nanocrystalline TiO_2 and ZnO, Sci. Total Environ. 485 (2014) 263–269.

[46] Y.F. Rao, W. Chu, Y.R. Wang, Photocatalytic oxidation of carbamazepine in triclinic-WO_3 suspension: role of alcohol and sulfate radicals in the degradation pathway, Appl. Catal. A-Gen. 468 (2013) 240–249.

[47] X.Y. Gao, X.C. Zhang, Y.W. Wang, S.Q. Peng, B. Yue, C.M. Fan, Photocatalytic degradation of carbamazepine using hierarchical BiOCl microspheres: some key operating parameters, degradation intermediates and reaction pathway, Chem. Eng. J. 273 (2015) 156–165.

[48] C. Martinez, M.Canle L, M.I. Fernandez, J.A. Santaballa, J. Faria, Kinetics and mechanism of aqueous degradation of carbamazepine by heterogeneous photocatalysis using nanocrystalline TiO_2, ZnO and multi-walled carbon nanotubes-anatase composites, Appl. Catal. B-Environ. 102 (3–4) (2011) 563–571.

[49] L.L. Bo, K.B. He, N. Tan, B. Gao, Q.Q. Feng, J.D. Liu, L. Wang, Photocatalytic oxidation of trace carbamazepine in aqueous solution by visible-light-driven Znln(2)S (4): performance and mechanism, J. Environ. Manage. 190 (2017) 259–265.

[50] M. Nawaz, W. Miran, J. Jang, D.S. Lee, One-step hydrothermal synthesis of porous 3D reduced graphene oxide/TiO_2 aerogel for carbamazepine photodegradation in aqueous solution, Appl. Catal. B-Environ. 203 (2017) 85–95.

[51] C.S. Pan, J. Xu, Y.J. Wang, D. Li, Y.F. Zhu, Dramatic activity of C_3N_4/$BiPO_4$ photocatalyst with core/shell structure formed by self-assembly, Adv. Funct. Mater. 22 (7) (2012) 1518–1524.

[52] S. Selvarajan, P. Malathy, A. Suganthi, M. Rajarajan, Fabrication of mesoporous $BaTiO_3$/SnO_2 nanorods with highly enhanced photocatalytic degradation of organic pollutants, J. Ind. Eng. Chem. 53 (2017) 201–212.

[53] W. Chen, Y.X. Hua, Y. Wang, T. Huang, T.Y. Liu, X.H. Liu, Two-dimensional mesoporous g-C_3N_4 nanosheet-supported $MgIn_2S_4$ nanoplates as visible-light-active heterostructures for enhanced photocatalytic activity, J. Catal. 349 (2017) 8–18.

[54] M.T. Qamar, M. Aslam, Z.A. Rehan, M.T. Soomro, J.M. Basahi, I.M.I. Ismail, T. Almeelbi, A. Hameed, The influence of p-type Mn_3O_4 nanostructures on the photocatalytic activity of ZnO for the removal of bromo and chlorophenol in natural sunlight exposure, Appl. Catal. B Environ. 201 (2017) 105–118.